Momentum Redistribution Times of Resonantly Photogenerated 2D Excitons

R. Duer, I. Shtrichman, D. Gershoni, and E. Ehrenfreund

Department of Physics and Solid State Institute, Technion-Israel Institute of Technology, Haifa 32000, Israel

(Received 12 July 1996)

We apply a novel transient interband-pump intersubband-probe technique to directly measure the time it takes for resonantly photoexcited excitons in GaAs/AlGaAs quantum well structures to redistribute in momentum space. The redistribution time and its excitation density dependence are determined from the temporal evolution of the conduction intersubband absorption spectrum, which is an unambiguous measure of the electrons phase space distribution. We find that resonantly excited heavy-hole excitons redistribute and reach thermal distribution at a slow rate nearly proportional to their density. This is due to the inefficient exciton-exciton scattering, and the small momentum that resonantly excited excitons carry. [S0031-9007(97)03187-6]

PACS numbers: 71.35.–y, 78.47.+p, 78.66.Fd

The dynamics of carriers in semiconductor quantum structures has been the subject of intensive research efforts in recent years. Following resonant and nonresonant optical excitation the photoexcited electrons, holes, and excitons are interacting with each other and gradually change their initial energy, momentum, and relative phase. The processes by which photogenerated excitons lose their initial coherence and redistribute in momentum space are exciton-exciton scattering (X-X), exciton-electron scattering (X-e), exciton-hole scattering, scattering by interaction with free electron-hole pairs, and scattering by crystal imperfections, interface roughness, and potential fluctuations. In addition, a two dimensional (2D) exciton with an in-plane momentum smaller than the momentum of the photon of the same energy, can decay radiatively within a few tens of picoseconds [1]. These processes have been extensively studied using time resolved photoluminescence (PL) [2–4], absorption [5], and nonlinear optical techniques [6,7]. From these measurements, X-X scattering times were found to be approximately 1 ps for excitation densities of $\simeq 1 \times 10^{10}$ cm^{-2} and inversely proportional to the excitation densities [6–8]. This time was recently found to be roughly a factor of 2 longer than X-e scattering times at comparable densities [7].

A common feature to all these time resolved optical techniques is the use of an interband optical probe, which is associated with the creation and/or annihilation of an electron-hole pair with a very small total crystal momentum. Such a probe provides only indirect information about the phase space distribution of the carriers. In addition, exciting and probing at the same optical resonance is a major technical problem due to the immense background from the scattered light. In an attempt to overcome these problems we have recently developed a novel time resolved interband-pump intersubband-probe technique [9]. Our technique uses a mid infrared (ir) probe pulse resonantly tuned to optical transitions of carriers between their subbands. The tuning of the probe pulse is completely independent of the pump pulse, which can be simultaneously tuned through the interband resonances. In contrast with the interband probe, the intersubband probe pulse does not create an electron-hole pair, but rather induces an optical transition (almost vertical in momentum space) of only one type of photoexcited carrier (electron or hole). As a result, the probe pulse is not subjected to the exclusion principle and it is extremely sensitive to the momentum state of the carrier whose optical transition is being induced. By tuning the probe energy through the conduction intersubband absorption (ISBA) line and measuring the relative strength, a direct measurement of the population of electrons in various momentum states within the first conduction subband can be obtained, provided that a correlation can be made between the transition energy and the electron momentum.

In this Letter we report on time resolved photoinduced ISBA measurements performed on a GaAs/AlGaAs superlattice (SL). The SL was specifically designed such that its first electronic level ($e1$) has almost no dispersion, while the second electronic level ($e2$) is considerably dispersed along the growth axis. In this way a simple correlation can be drawn between the intersubband transition energy and the momentum states of the electron excited from $e1$ to $e2$. The evolution of this SL intersubband absorption spectrum with the delay time between the pump and the probe, provides an unambiguous tool for the determination of the momentum redistribution of electrons after resonant photoexcitation into the lowest energy excitonic transition. In a larger period SL or a multi quantum well, such a correlation is quite difficult to be drawn since the spectral linewidth of its conduction intersubband optical transitions is narrower. At low temperatures it results mainly from the dissimilarity between the subbands in-plane dispersion [10] and the growth nonuniformity and well width fluctuations [11]. Indeed, in such samples, as opposed to the data presented here, we have not observed temporal evolution of the intersubband absorption spectrum [12].

The superlattice was grown by molecular beam epitaxy on a (100)-oriented GaAs substrate and consists of 33

nominally undoped periods of 91 Å thick $Al_{0.33}Ga_{0.67}As$ layer followed by a 49 Å thick GaAs layer. The layer thicknesses and their composition were determined by high resolution x-ray diffraction measurements. A schematic description of the SL conduction band potential structure is given in Fig. 1(b). The calculated energy dispersion vs the electronic crystal momentum components along the SL axis k_z^e and in the layer planes $k_\parallel^e$ are given in Figs. 1(a) and 1(c), respectively. We use an eight band $\mathbf{k}\cdot\mathbf{p}$ model for the calculations of the energies, the wave functions, and the optical transition matrix elements of carriers in this structure [13]. With these quantities at hand, the intersubband absorption spectrum is readily calculated once the number of electrons and their momentum space distribution are known [13]. Because of the considerable dispersion of $e2$ along the k_z^e axis the ISBA spectral shape can be used as a quantitative measure for the phase space distribution of the photoexcited electron population in $e1$.

The time resolved photoinduced absorption (PIA) setup consists of three synchronously pumped picosecond dye lasers. All three are simultaneously pumped by a frequency doubled CW mode-locked Nd:YAG laser. The pulses from one of the dye lasers are used to excite the sample, while the pulses from the other two are difference frequency mixed within a silver thiogallate crystal to produce the tunable IR probe pulse. The IR pulse can be variably delayed relative to the pump pulse, and the changes in the IR transmission through the sample due to the excitation are detected by a liquid nitrogen cooled mercury cadmium telluride detector and a conventional lock-in technique. This setup allows for pump-probe visible-IR time resolved spectroscopy with a temporal resolution of 3–4 ps and spectral resolution of a few tenths of meV, both in the pump and probe energies [9]. For the intersubband PIA spectroscopy, the sample was cleaved and polished at 45° to the growth axis in order to form a waveguide for the ir radiation and to enable a considerable electric field component along the growth axis. The geometry of the experiment is described in the inset to Fig. 2. The measurements were done with the sample mounted on a cold finger assembly in a helium transfer cryostat.

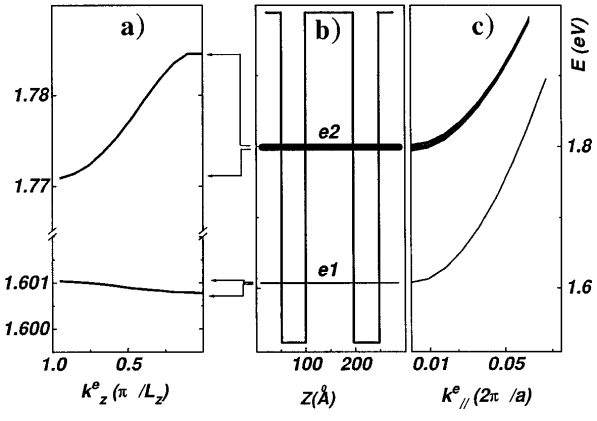

FIG. 1. The supperlattice conduction band potential structure (b) and its calculated dispersion curves along the growth axis (a) and in the layers plane (c). Note the different energy scales in (a).

In Fig. 2 we display the PIA intensity under HH (a) and LH (b) resonant excitations vs the pulsed, p-polarized, ir probe energy for various pump-probe delay times. The data points were taken one by one as indicated by the full squares. The time resolved PIA spectra are vertically displaced for clarity and the zero intensity of each spectrum is represented by a horizontal solid line. The solid lines overlaid over the 2 and 30 ps delay spectra [Fig. 2(a)] are the calculated ISBA assuming resonant and thermal distribution of the photogenerated excitons, respectively (see below). The density of $\simeq 1 \times 10^{11}$ cm^{-2} excitons per period was estimated from the measured beam average power, repetition rate, and spot diameter on the sample. The calculated absorption was multiplied by the period length and by the number of periods in order to facilitate direct comparison with the measured data. In general, we find a very good agreement between the calculated intensity of the ISBA and the measured time resolved PIA spectra at $\simeq$70 ps delay, after thermal equilibrium between the photoexcited carriers and the

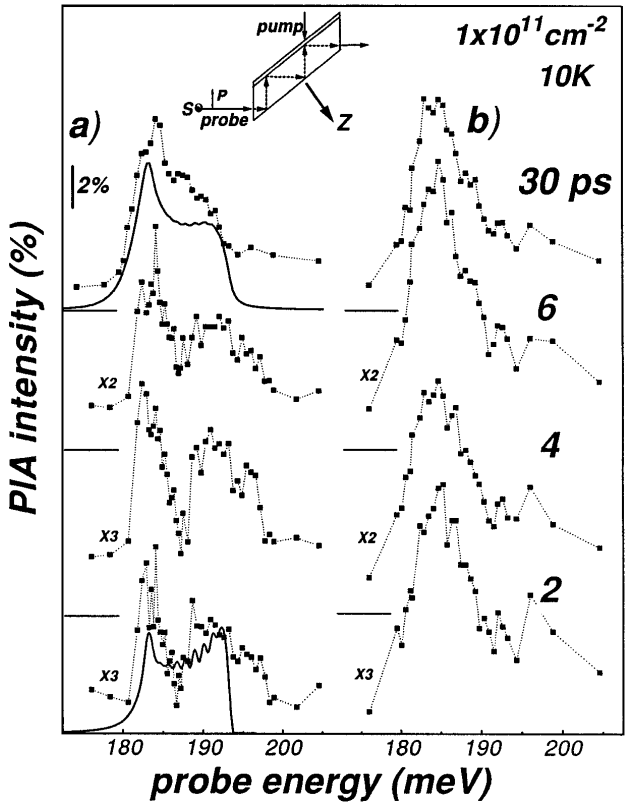

FIG. 2. Time resolved PIA spectra at resonance excitation into (a) HH exciton (b) LH exciton. The overlaid solid lines represent the calculated ISBA with electrons in thermal distribution at 10 K (30 ps delay), and in a nonthermal distribution at the moment of photogeneration (2 ps delay).

ambient crystal is reached. Up to this time, which is temperature and excitation energy dependent [9,14] the PIA intensity keeps increasing as shown in Fig. 2. Both the calculated and measured spectra feature a pronounced peak at $\simeq$184 meV and a higher energy shoulder at $\simeq$190 meV. As can be seen in Fig. 1(a), these spectral features correspond to the singular points in the $e1$-$e2$ joint density of states at $k_z^e = \pi/L_z$ and $k_z^e = 0$, respectively, where L_z is the SL period length.

For resonantly excited HH excitons, the relative intensity of the high energy shoulder at $\simeq$190 meV evolves with time as shown in Fig. 2(a). Within the picosecond excitation pulse it is comparable in intensity to the low energy peak at 184 meV. It then loses its relative strength and the spectrum reaches its final shape, after approximately 30 ps, an unambiguous indication that thermal distribution of the photoexcited carriers has been reached. The strength of the high energy shoulder in the ISBA spectrum is thus a quantitative measure for the phase space distribution of the photoexcited electron population in $e1$ *before* it reaches thermal distribution. For the case of resonantly excited LH excitons, Fig. 2(b), no temporal evolution of the ISBA spectrum is seen. Very similar temporal behavior is observed also for other off HH exciton resonance excitations. We attribute these observations to very fast scattering processes which take place when excitons are not the only photogenerated species. Then, the redistribution processes are apparently faster than our temporal resolution (see below). The difference between the 30 ps ISBA spectra of the HH and LH resonant excitations is due to almost a factor of 2 higher photogenerated carrier density in the latter case, where the optical absorption is stronger.

In Figs. 3(a) and 3(b) we present the calculated electron densities as a function of their momenta k_z^e and $k_\parallel^e$ at resonant excitation, and at 10 K thermal distribution, respectively. These distributions were used for the calculations of the ISBA spectra overlaid the 2 and 30 ps delay spectra in Fig. 2(a), respectively. For these calculations we note that the electronic crystal momentum is given in terms of the exciton center of mass and relative momenta: $\mathbf{k^e} = \mathbf{K}/2 + \mathbf{k}$, where $\mathbf{K}$ and $\mathbf{k}$ are the exciton center of mass and relative momenta, respectively [15]. The relative momentum $\mathbf{k}$ distribution is estimated from the Fourier transform of the $1s$ $e1$-HH1 excitonic envelope wave function. The exciton envelope wave function in these quantum wells is assumed to be a three dimensional ellipsoid [16] whose axes (65 Å in-plane and 33 Å along the growth direction) are determined by a simple one band variation model. The Fourier transform of this envelope wave function, convoluted with half the excitonic momentum $\mathbf{K}$ distribution, yields the electrons phase space distribution. For resonant photoexcitation into the HH excitonic resonance the electron phase space distribution is given approximately by the relative momentum $\mathbf{k}$ distribution, since the exciton momentum $\mathbf{K}$ is very small.

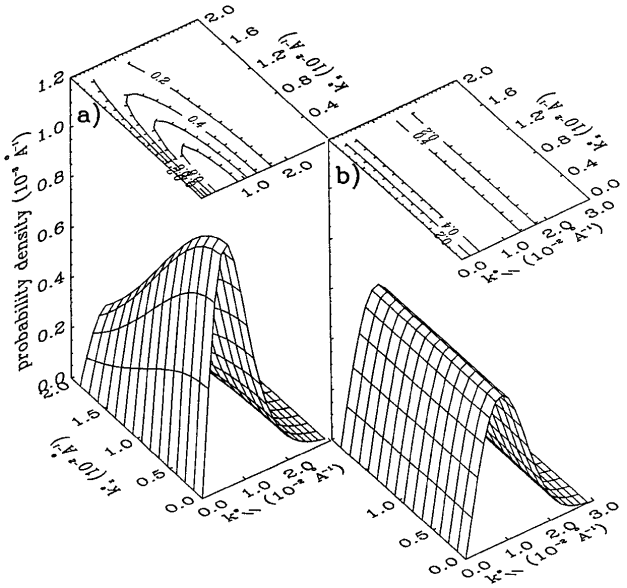

FIG. 3. The calculated phase space probability density of electrons for resonantly photogenerated excitons (a), and for 10 K thermally distributed excitons (b).

This distribution, integrated over the azimuthal in-plane angle in momentum space, is depicted in Fig. 3(a), where it can be seen that low k_z^e states are heavily populated, whereas high k_z^e states are suppressed by nearly a factor of 4. This nonthermal distribution results in a considerable enhancement of the high energy shoulder in the ISBA spectrum, which is due to $e1$ electron states at $k_z^e \simeq 0$, as given by the solid line overlaid on the measured 2 ps time resolved ISBA spectrum in Fig. 2(a) [17]. After thermal distribution is reached, the situation is markedly different. Now the excitons momentum $\mathbf{K}$ distribution significantly affects the electrons momentum distribution. At the measurement temperature, where the thermal energy is much smaller than the excitonic binding energy, the in-plane momentum distribution is still mainly determined by the excitonic relative momentum. However, since the dispersion of the electrons (and excitons) along the growth direction is much smaller than the thermal energy, electrons are now evenly distributed along the k_z^e axis. This distribution is depicted in Fig. 3(b). The resulted ISBA line shape is mainly determined by the $e1$-$e2$ joint density of states as given by the solid line overlaid on the measured 30 ps time resolved ISBA spectrum in Fig. 2(a).

In Fig. 4 we show the excess intensity (above the intensity after thermal distribution has arrived at) of the high energy shoulder relative to the intensity of the whole ISBA line as a function of the probe delay for various pump intensities. Single experimental decay models best fitted to the experimental data are given in the figure by solid lines. We use this procedure for extracting a characteristic time constant for the momentum redistribution from the experimental data. We note

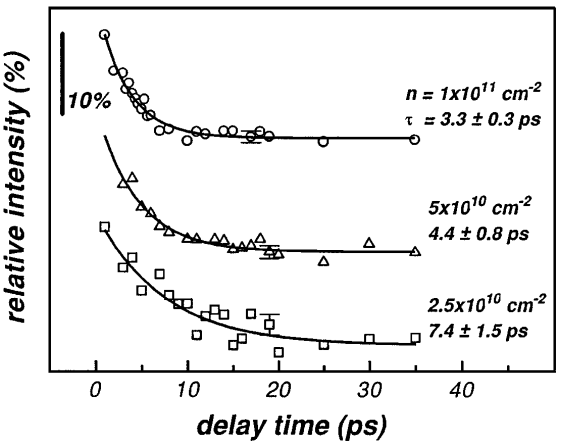

FIG. 4. The relative intensity of the high energy shoulder (the 190 meV region) as a function of the probe delay at three different pump intensities. The solid lines are single exponential decay fits; the decay times are marked on the figure.

that for low exciton densities 2.5×10^{10} cm^{-2}, thermal distribution is reached within $\simeq$8 ps. This time is almost inversely proportional to the excitation density, as expected for *X*-*X* scattering processes [6–8].

The redistribution time of resonantly photogenerated 2D excitons which we have obtained by a direct measurement is almost an order of magnitude longer than the measured *X*-*X* scattering time [7,8]. This difference should not come as a surprise. The momentum exchange during *X*-*X* interaction cannot exceed the momentum that a resonantly photogenerated exciton carries. This momentum amounts only to $k_0 = 2\pi n/\lambda \simeq 2.4 \times 10^{-3}$ Å^{-1}, where n is the material index of refraction and λ is the wavelength of the photon in vacuum. This is an order of magnitude smaller than the crystal momentum associated with the low energy peak in the ISBA spectrum: $k_z^e = \pi/L_z = 2.2 \times 10^{-2}$ Å^{-1}. Thus, many more than a single *X*-*X* interaction event are required in order for the momentum space redistribution to take place. Though the detailed dynamics involved in this momentum redistribution is beyond the scope of this Letter, we find it plausible that the above momenta ratio is comparable to the ratio between the *X*-*X* scattering time and the redistribution times that we have measured here for the first time.

For resonant excitation into the LH exciton the situation is different [Fig. 2(b)]. Here, not only excitons are generated, but electrons and holes with excess energy of a few meV are generated as well. Carrier-carrier and carrier-exciton scattering processes are known to be faster than exciton-exciton scattering processes. Moreover, photogenerated carriers can carry with them larger momentum quanta than photogenerated excitons. Thus phase space redistribution takes place on a much faster time scale which is below our temporal resolution [5]. Consequently, for this and other nonresonant pump energies, no temporal evolution could be seen.

In summary, we have shown that resonantly photogenerated excitons which carry with them very small crystal momentum at the time of creation, redistribute in phase space and reach thermal distribution on a few ps time scale, inversely proportional to their areal density. We attribute this time scale, which is much longer than the previously measured single *X*-*X* scattering process, to multiple *X*-*X* scattering events, required to complete the phase space redistribution.

This work was supported by the Israel Science Foundation administered by the Israeli Academy of Sciences and Humanities. We thank P. M. Platzman, D. S. Chemla, and U. Sivan for stimulating discussions.

[1] L. C. Andreani, Solid State Commun. **77**, 641 (1991).
[2] J. Feldman *et al.,* Phys. Rev. Lett. **59**, 2337 (1987).
[3] B. Deveaud *et al.,* Phys. Rev. Lett. **67**, 2355 (1991).
[4] A. Vinattieri *et al.,* Solid State Commun. **88**, 189 (1993).
[5] W. H. Knox *et al.,* Phys. Rev. Lett. **56**, 1191 (1986).
[6] L. Schultheis, L. Kuhl, A. Honold, and C. W. Tu, Phys. Rev. Lett. **57**, 1635 (1986).
[7] M. Koch *et al.,* Phys. Rev. B **51**, 13 887 (1995).
[8] H. Wang, J. Shah, T. C. Damen, and L. N. Pfeiffer, Phys. Rev. Lett. **74**, 3065 (1995).
[9] R. Duer, D. Gershoni, and E. Ehrenfreund, Supperlattices Microstruct. **17**, 5 (1995).
[10] J. Oiknine-Schlesinger *et al.,* Appl. Phys. Lett. **59**, 970 (1991).
[11] D. Gershoni *et al.,* Phys. Rev. Lett. **71**, 2975 (1993).
[12] D. Gershoni *et al.,* in *Applied Sciences,* NATO ASI, Ser. E, Vol. 270 (Kluwer Academic Publishers, 1994), p. 275.
[13] D. Gershoni, C. H. Henry, and G. A. Baraff, IEEE J. Quantum Electron. **29**, 2433 (1993).
[14] R. Eccleston *et al.,* Phys. Rev. B **45**, 11 403 (1992).
[15] R. J. Elliott, Phys. Rev. **108**, 1384 (1957).
[16] P. Christol, P. Lefebvre, and H. Mathieu, J. Appl. Phys. **74**, 5626 (1993).
[17] Note that these calculations still neglect the influence of the exciton Coulomb attraction on the second $e2$ electronic subband. Using a single band variational model we have found that inclusion of the excitonic interaction, should slightly affect the optical matrix elements used for the calculation of the absorption spectra. This should not affect the physical picture described here.